Characteristics of mixed-phase clouds. II: A climatology from ground-based lidar

By R. J. HOGAN[1]*, A. J. ILLINGWORTH[1], E. J. O'CONNOR[1] and J. P. V. POIARES BAPTISTA[2]
[1]*Department of Meteorology, University of Reading, UK*
[2]*ESA/ESTEC, Noordwijk, the Netherlands*

SUMMARY

In part I it was demonstrated that supercooled liquid-water clouds can occur in the form of thin but radiatively significant layers that are distinctive in lidar imagery due to their high backscatter coefficient. In this paper, 18 months of near-continuous lidar data from two midlatitude locations are analysed to estimate the frequency of occurrence of such clouds as a function of temperature. An algorithm is developed that uses the integrated backscatter to identify liquid-water clouds with a visible optical depth of greater than 0.7 (i.e. those that scatter more than half of the incident radiation), and is found to compare favourably with microwave-radiometer measurements of liquid-water path. From data taken with a lidar pointing at 5° from zenith, the frequency of supercooled liquid-water layers over Chilbolton in southern England is found to fall steadily with temperature; 27% of clouds between $-5\,°C$ and $-10\,°C$ are found to contain significant liquid water, falling to only 6% of clouds observed between $-25\,°C$ and $-30\,°C$. The horizontal extent of the layers typically ranges between 20 and 70 km. When the lidar is pointed directly at zenith, specular reflection by horizontally aligned plate crystals is found to bias the statistics between $-10\,°C$ and $-20\,°C$. The importance of supercooled liquid-water clouds in the radiation budget is reduced when thick ice clouds are present above them, so we then use simultaneous cloud radar data to estimate the optical depth of any cloud above. It is found that around 30% of supercooled liquid-water clouds with temperatures between $0\,°C$ and $-20\,°C$ have ice above with a visible optical depth in excess of 0.5, falling to 10% between $-20\,°C$ and $-30\,°C$. Given the substantial optical depth of the supercooled water itself, we conclude that in the majority of cases when supercooled water is present, it will dominate the radiative properties of the cloud profile. Finally, we compare the occurrence of supercooled-liquid clouds with the amounts found in the models of the UK Met Office and the European Centre for Medium-Range Weather Forecasts (ECMWF). Both models are found to produce too much supercooled liquid at warmer temperatures and too little at colder temperatures (with virtually none being simulated below $-20\,°C$), although the occurrence of supercooled cloud is far higher in the ECMWF model than the Met Office model. The observations in this paper are limited to one climatic zone but the forthcoming spaceborne lidars will be able to extend these comparisons to the whole globe.

KEYWORDS: Backscatter lidar   Integrated backscatter   Specular reflection   Supercooled water

1. INTRODUCTION

Despite the potential importance of mixed-phase clouds in the climate system (e.g. Sun and Shine 1995; Gregory and Morris 1996), the lack of good observational datasets has meant that cloud-phase parametrizations in numerical forecast and climate models have tended to remain rather crude, involving typically a single prognostic variable for cloud water content that is divided into liquid and ice on the basis of temperature alone. Some recent, more physically based parametrizations use other model variables (such as vertical velocity) to aid the diagnosis of liquid/ice fraction (Tremblay *et al.* 1996), while others go further and use separate prognostic variables for ice and liquid water (Wilson and Ballard 1999). Clearly, long-term observations from the ground and from space are needed, both for direct evaluation of model forecasts, and to build up a climatology against which climate models may be tested.

Satellite measurements of supercooled clouds have been reported from the Polarization and Directionality of the Earth Reflectances (POLDER) instrument on board the

* Corresponding author: Department of Meteorology, Earley Gate, PO Box 243, Reading, Berkshire RG6 6BB, UK. e-mail: r.j.hogan@reading.ac.uk

Advanced Earth Observing System (ADEOS) platform. Goloub *et al.* (2000) measured the polarization properties of reflected sunlight at up to 14 different angles, and identified the occurrence of liquid-water droplets by the presence of a sharp peak in the polarized radiance near the 'rainbow' angle of $140°$. Analysis of 120×10^6 km^2 of coincident Along-Track Scanning Radiometer (ATSR)-2 infrared data obtained on a single day by Giraud *et al.* (2001) suggested that the probability of a cloud being composed of ice was a quasi-linear function of cloud-top temperature, falling from nearly 100% at around $-33\,°$C to close to 0% at $-10\,°$C. Conversely, Riedi *et al.* (2001) compared the POLDER retrieval with the cloud-top temperature derived using radar and lidar on the 201 days that the instrument flew over the Atmospheric Radiation Measurement (ARM) site in Oklahoma, and found a sharp transition from purely liquid to purely ice at $-33\,°$C.

In part I (Hogan *et al.* 2003b) it was shown that supercooled liquid-water clouds can occur in the form of thin layers, around 150 m thick, that are distinctly visible to lidar due to their very high backscatter coefficient. By contrast, the echo from a cloud radar tends to be dominated by the contribution from the larger but much less numerous ice particles. The phase of the layers was confirmed by both their low lidar depolarization and the *in situ* aircraft measurements. In this paper we use around 8 months of near-continuous data taken by a 905 nm Vaisala lidar ceilometer located at Chilbolton, England, and 10 months of data from an identical instrument at Cabauw, the Netherlands, to estimate the frequency of occurrence of supercooled clouds as a function of temperature. These instruments do not have polarization capability, and although depolarization ratio is perhaps the most well known method to detect cloud-particle phase remotely (Sassen 1991), the high backscatter coefficient of the layers combined with their rapid extinction of the lidar signal makes them quite easy to detect using a simple backscatter lidar. An algorithm is developed which utilizes the integrated backscatter coefficient through the candidate layer; due to the approximately constant extinction-to-backscatter ratio of distributions of liquid-water droplets with median diameters in the range 5–50 μm, this can be used to impose a lower limit on the optical depths that are detected. Importantly, the Vaisala instrument is able to operate continuously in all weather conditions, an essential consideration if a representative climatology is to be built up. Of course, there may be considerable regional variability to the characteristics of mixed-phase clouds, but this paper demonstrates a methodology that could be applied to other lidars, both from the ground and from space.

Radiative-transfer calculations were performed in part I to estimate the radiative importance of the supercooled liquid-water layers observed and it was found that in each profile analysed the effect of the liquid water on the net top-of-atmosphere radiation was greater than that of the ice. In principle, however, thick cirrus could swamp the radiative signature of the liquid-phase cloud beneath. The thickest cirrus considered in part I had an optical depth of 0.78, and caused a reduction in outgoing long-wave radiation of 65.7 W m^{-2}, much larger than the 25.2 W m^{-2} due to the liquid water below. However, the increase in reflected short-wave radiation due to the ice was less than that due to the liquid water, with the result that the liquid water still had a significantly greater effect on the *net absorbed* radiation than the ice (-83.9 W m^{-2} as opposed to -18.2 W m^{-2}). To determine how often thick cirrus occurs in conjunction with supercooled clouds, we use the vertically pointing 94 GHz Galileo radar at Chilbolton, which also operates near-continuously, to estimate the optical depth of any cirrus whenever the lidar detects a supercooled liquid-water cloud.

Several lidar studies of cirrus (Gibson *et al.* 1977; Platt *et al.* 1978; Sassen 1984; Thomas *et al.* 1990) have found cases of ice clouds that exhibit enhanced backscatter

when viewed from zenith, up to a factor of 20 higher than the backscatter measured when the lidar is pointed only a few degrees to the side. This can be explained by the presence of horizontally oriented plate crystals that undergo specular reflection when viewed from directly below. These are the same crystals that reflect sunlight preferentially in particular directions to produce certain optical phenomena. From the angular dependence of the backscatter, Thomas *et al.* (1990) estimated the maximum tilt of the crystals from the horizontal plane to be around $0.3°$. Unlike in the case of supercooled-water layers, the enhanced backscatter due to aligned plates is not accompanied by a strong increase in extinction, but there is still a danger that specular reflection could be mistaken for supercooled water. We, therefore, use data taken at $5°$ from zenith to determine the frequency of occurrence of liquid-water layers, and compare these results with data taken at zenith to estimate the prevalence of specular reflection in ice clouds. It should be noted that the specular component of reflection from plate crystals is not depolarized, so the depolarization ratio does not provide a means to distinguish specularly reflecting ice crystals from liquid-water droplets.

In section 2 the lidar and radar instruments are described, including details of their calibration. In section 3 we describe the algorithm used to diagnose the presence of liquid water with lidar and the methodology for using simultaneous radar data to estimate the optical depth of any ice cloud above. The results are then presented in section 4, including comparison of the observed occurrence of supercooled-water clouds with the amounts in the models of the UK Met Office and the European Centre for Medium-Range Weather Forecasts (ECMWF).

2. INSTRUMENTATION

The main instrument used in this paper is the 905 nm Vaisala CT75K lidar ceilometer, which has a range gate spacing of 30 m and obtains improved sensitivity, despite its low power, by integrating for 30 s. The Chilbolton lidar has operated continuously since January 1997, except for a few periods off-line for maintenance. It was originally set up in a zenith-pointing configuration, but in December 1999 was adjusted to point at $5°$ from zenith; data both with and without contamination from specular reflection are therefore available. We also use data from an identical instrument operating at $5°$ from zenith at Cabauw, the Netherlands, between October 2001 and July 2002. The lidars have been calibrated by integrating the raw attenuated backscatter coefficient up through completely attenuating stratocumulus*. Theoretically this integral should be equal to $(2\eta k)^{-1}$, where η is the multiple-scattering factor and k is the extinction-to-backscatter ratio (Platt 1973). In the next section it is shown that these parameters can be assumed constant in the type of clouds under consideration.

The optical depth of the ice clouds above the supercooled liquid water is estimated using the 94 GHz Galileo radar at Chilbolton. This instrument operated near-continuously in a vertically pointing configuration between November 1998 and October 2000. Calibration has been performed regularly by comparison with the 3 GHz radar at Chilbolton, as described by Hogan *et al.* (2003a), and is believed to be accurate to better than 1.5 dB. It was found that the power emitted by the instrument decreased steadily by 11 dB in these two years of operation. The last 94 GHz data used in this paper, from October 2000, had a minimum detectable radar reflectivity of around -39 dBZ at 1 km.

---

* The calibration technique is described fully by O'Connor *et al.* (document in preparation).

3.   METHOD

(*a*)   *Objective diagnosis of the presence of supercooled liquid water*

In this section we describe the algorithm used to detect the presence of supercooled water. The technique essentially locates highly reflective layers in the lidar imagery that, on the basis of the observations in part I, have a backscatter coefficient that is too high to be likely to be caused by ice alone. By utilizing the integrated backscatter coefficient, it is possible to accurately specify the optical depth that will trigger the algorithm. This approach was first suggested by Platt (1973) and was used by him in the study of clouds in numerous subsequent papers.

The lidar measures attenuated backscatter coefficient β', which is related to true backscatter coefficient β by

$$\beta'(z) = \beta(z)\, e^{-2\eta\tau(z)}, \tag{1}$$

where $\tau(z)$ is the optical depth of the atmosphere at 905 nm between the instrument and the point of observation at height z. This equation follows Platt (1973) in its representation of multiple scattering by a single factor η, which can take a value between 0.5 and 1 depending on the parameters of the lidar and the nature of the scatterers in the cloud.

In each lidar profile, the algorithm determines the height of the highest value of β' and then calculates the integrated backscatter through this 'candidate' liquid-water layer, γ_w, defined by

$$\gamma_w = \int_{z_1}^{z_2} \beta'\, dz, \tag{2}$$

where z_1 is 100 m below the height of the highest β' and z_2 is 200 m above the height of the highest β'. It is our experience that, due to their strong attenuation, individual liquid-water layers tend to occupy no more than 300 m of a lidar profile, and that z_1 and z_2 defined in this way encapsulate liquid-water layers most effectively. Noting that extinction coefficient α is equal to $d\tau/dz$, and assuming the extinction-to-backscatter ratio, $k = \alpha/\beta$, to be constant through the cloud, we can change variables and write

$$\gamma_w = \frac{1}{k}\int_{\tau_1}^{\tau_1+\tau_w} e^{-2\eta\tau}\, d\tau$$

$$= \frac{1}{2\eta k}\, e^{-2\eta\tau_1}(1 - e^{-2\eta\tau_w}), \tag{3}$$

where τ_w is the optical depth of the candidate liquid-water layer and τ_1 is the optical depth of the atmosphere from the surface to z_1.

In the simple case of the lidar having an unobscured view of the liquid-water layer ($\tau_1 \simeq 0$) and the layer being optically thick ($\tau_w \to \infty$), Eq. (3) reduces to $\gamma_w = (2\eta k)^{-1}$. Using complex angular-momentum theory at a wavelength of 1.06 μm, Pinnick *et al.* (1983) calculated that for droplet distributions typically found in liquid-water clouds, k is approximately constant at 18.2 sr. Using Mie theory at 905 nm and distributions with median volume diameters in the range 5–50 μm, we find that k is approximately constant at 18.75 sr. Using the code of Eloranta (1998) and realistic droplet size distributions observed at a range of at least 3 km, we calculate that for the CT75K lidar beam divergence (0.75 mrad half angle) and field of view (0.66 mrad half angle), η is approximately constant at 0.7 ± 0.04. Therefore, γ_w in optically thick liquid-water clouds is around 0.038 sr^{-1}.

We specify that the supercooled liquid-water clouds detected by the algorithm should have an optical depth τ_w greater than 0.7; i.e. that over half of the radiation incident normally on the cloud layer should be scattered. Thus, if it is still assumed that $\tau_1 \simeq 0$, then from Eq. (3) the condition for such a cloud to be detected is $\gamma_w > 0.024 \ sr^{-1}$. The fraction of clouds that contain a liquid-water layer in any given temperature interval may then be calculated by dividing the time for which γ_w exceeds this threshold and lies in the specified temperature interval, by the total time that any cloud is detected in this temperature range.

In reality there may be significant optical depth beneath a liquid-cloud layer, most commonly in the case of ice virga beneath an altocumulus layer, but aerosol attenuation could also be a factor. If uncorrected this could lead to an underestimate of the fraction of clouds containing a layer due to the reduction in measured γ_w. Since k is much less certain in ice than in liquid, we cannot reliably perform a gate-by-gate correction for attenuation. Instead, we simply remove cloudy pixels that have an optical depth beneath them high enough that they could never be diagnosed as being a liquid-water layer by the criterion of $\gamma_w > 0.024 \ sr^{-1}$. The cloud below the layer is assumed to have a k equivalent to the liquid-water value; this will sometimes remove too much cloud and sometimes too little, but as it is also a fairly typical value for ice, any bias should be small. This procedure removes around 20% of the cloudy pixels.

(b) Examples of mixed-phase clouds observed by ground-based radar, lidar and microwave radiometer

Figures 1 and 2 show cases of supercooled liquid water observed at Chilbolton. The first is from 6 August 1999 and depicts 12 h time–height sections of radar and lidar data. Superimposed on the lidar image are temperature contours from the mesoscale version of the operational Met Office Unified Model. The model dataset is hourly, composed of the 6-hourly analyses followed by the intervening hourly forecasts. In the lowest kilometre the lidar detects boundary-layer aerosol, while the radar echo is contaminated by returns from the ground and insects. Above this, at temperatures between $+10\ ^\circ$C and $-20\ ^\circ$C, a number of thin but highly reflective layers, believed to be composed of liquid water, are apparent in the lidar signal. They are very similar in appearance to the layers observed in part I, which depolarization measurements and *in situ* sampling confirmed to be composed of liquid water. For most of the time in Fig. 1 when a layer was observed at temperatures below $0\ ^\circ$C, the radar detected ice falling beneath it. Figure 1(b) depicts the integrated backscatter γ_w in a 300 m vertical window encompassing the strongest echo, with the values above the detection threshold of $0.024\ sr^{-1}$ shaded. The location of the diagnosed liquid-water layer is shown by the black points in Fig. 1(c), and in general matches the layers that might be identified subjectively on inspection of Fig. 1(a).

The second case is from 10 November 2001, when the clouds were almost entirely composed of liquid water and the radar (not shown) did not detect any cloud. The integrated backscatter in Fig. 2(b) shows that the cloud was, in general, optically thick. Figure 2(c) shows concurrent measurements of liquid-water path by a dual-wavelength microwave radiometer at 22.2 GHz and 28.8 GHz. The times that liquid water was detected agree well with the lidar measurements, with values reaching 150 g m^{-2}. However, it is interesting that there are optically significant liquid-water clouds apparent in the lidar data at around 0345 and 0800 UTC that have very low liquid-water paths and so are scarcely detected by the microwave radiometer. This is consistent with the finding in part I that supercooled-liquid clouds with a liquid-water path as low as 10 g m^{-1} can still have a significant radiative effect.
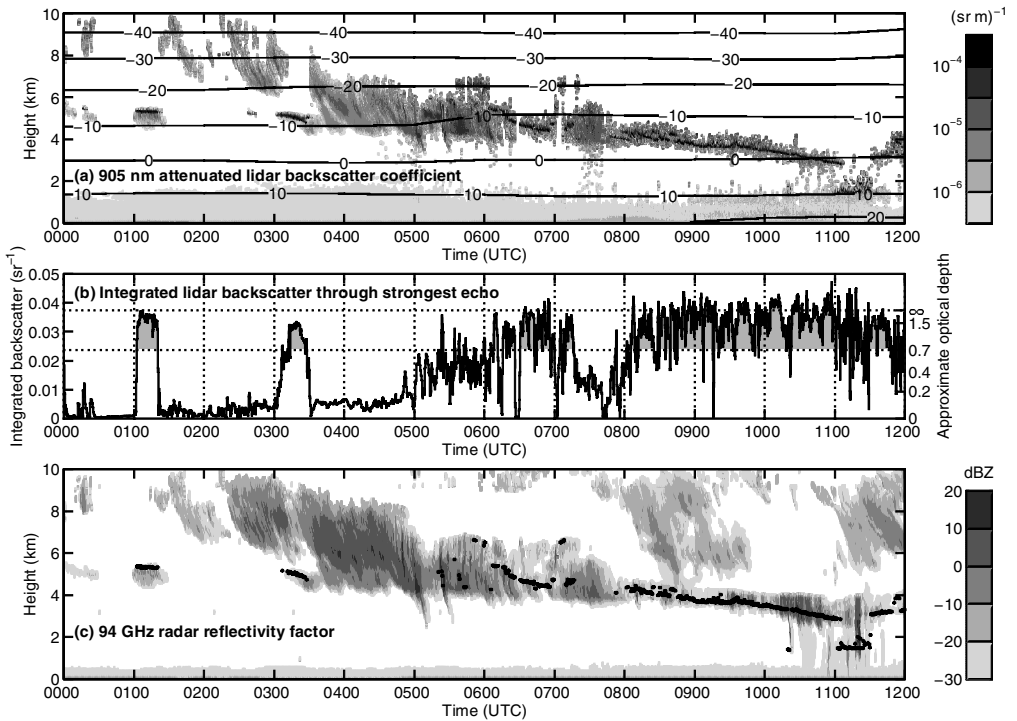
Figure 1.   Example of mixed-phase cloud detection on 6 August 1999 at Chilbolton: (a) 12 h time–height section of attenuated lidar backscatter coefficient, β', overlaid by temperature from the UK Met Office model ($°C$); (b) integrated attenuated backscatter coefficient in a 300 m window around the location of the highest β'; (c) attenuation-corrected 94 GHz radar reflectivity factor. The shaded areas of (b) indicate the presence of a liquid-water layer with an optical depth of more than 0.7, the location of which is shown by the black points in (c).

(c)   *Estimating the optical depth of ice cloud*

At Chilbolton, the visible extinction coefficient (α) of ice clouds may be estimated from the effective radar reflectivity factor (Z) measured by the 94 GHz cloud radar. This can then be integrated in height to estimate the optical depth (τ) of any ice cloud above the supercooled liquid water observed by the lidar. The first step is to correct the reflectivity values for attenuation. Correction of gaseous attenuation is performed using the temperature and humidity profile held over Chilbolton from the mesoscale version of the Met Office model, coupled with the line-by-line model for the millimetre-wave attenuation of Liebe (1985). The two-way liquid-water attenuation at 94 GHz is less than 0.01 dB $(g\,m^{-2})^{-1}$, so for the values of liquid-water path shown in Fig. 2 and in Table 1 of part I, the attenuation rarely reaches 1 dB and is often less than 0.1 dB. Of course, detection of supercooled liquid water by lidar implies that no thicker liquid-water cloud is present below, so we assume that liquid-water attenuation is negligible.

A relationship between Z and α was derived from a total of around 14 h of ice size-spectra measurements in midlatitude cirrus between $-2\,°C$ and $-57\,°C$ by the Met Office C-130 aircraft, taken predominantly during the European Cloud Radiation Experiment (EUCREX). It should be stressed that the ice under consideration in this paper is exclusively *above* the supercooled water, so is unlikely to be affected by it, justifying the use of a general cirrus dataset. Indeed, in the 20 October 1998 case of
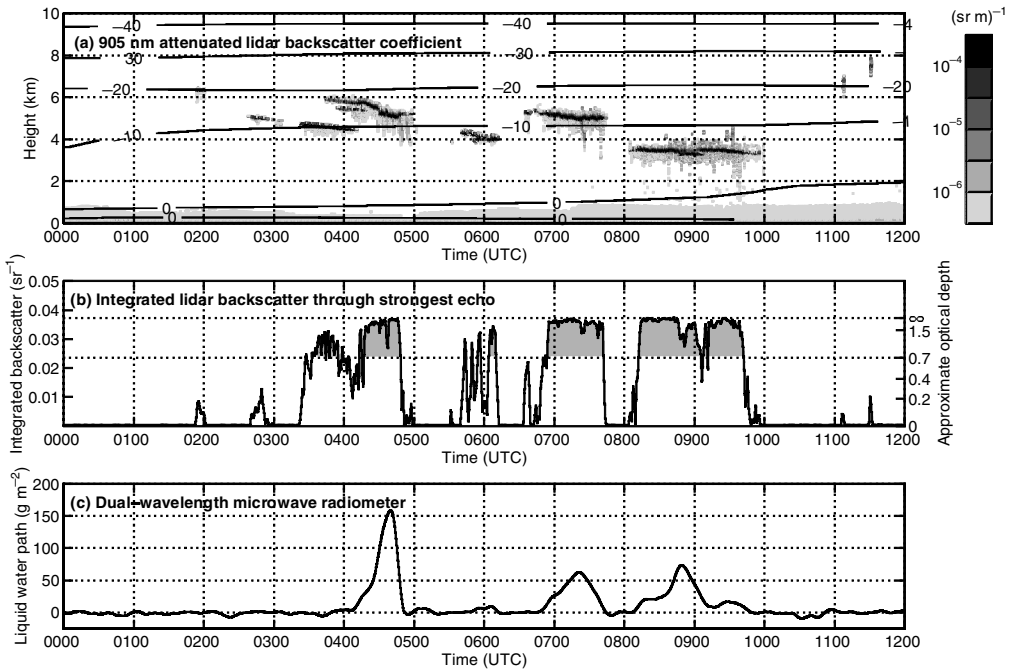
Figure 2.   Supercooled-water detection on 10 November 2001: (a) attenuated backscatter coefficient, (b) the approximate optical depth of the layer, as in Fig. 1, and (c) liquid-water path retrieved using a dual-wavelength microwave radiometer.

part I, most of the ice optical depth was in the cirrus which had a base 3 km higher than the highest liquid-water layer.

Radar reflectivity factor is calculated using the same approach as Brown *et al.* (1995) and Hogan and Illingworth (1999); the ice particles observed by the two-dimensional (2D) probes of the C-130 (spanning the diameter range 25–6400 μm) are approximated as spheres with a mass given by the relationship of Brown and Francis (1995) and a diameter, D_m, equal to the mean of the maximum dimensions of the particle measured parallel and perpendicular to the photodiode array of the probe. Then Mie theory is applied. Extinction coefficient is calculated directly from the observed cross-sectional area of the crystals assuming geometric optics. To account for the under-counting of the small particles by the 2D cloud probe, we take a similar approach to Francis *et al.* (1998) and fit a gamma distribution to the lower end of each size spectrum. The gamma distribution is constrained to have a modal diameter of 6 μm, to have the same concentration of 100 μm particles as observed, but twice as many 25 μm particles. This increases the ice-water content contained in the particles smaller than 90 μm by around a factor of 2.5, thereby correcting for the average difference that McFarquhar and Heymsfield (1997) found when they compared the 2D cloud probe to the video ice-particle sampler.

The data are shown in Fig. 3, where each point represents a 5 s aircraft sample. Simple regressions in logarithmic space can result in biased retrievals when the scatter of the data is large. To avoid this problem we first compute the linear mean of α in each 2 dB radar-reflectivity interval between -25 and $+5$ dBZ (shown by the diamonds) and then perform a linear regression in logarithmic space to these means. The resulting
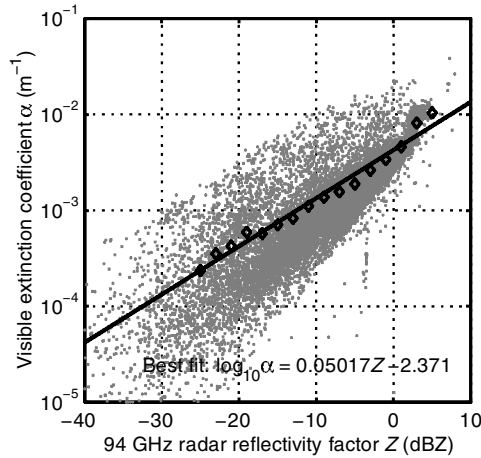
Figure 3. Scatterplot of radar reflectivity Z versus visible extinction coefficient α derived from the European Cloud Radiation Experiment (EUCREX) aircraft dataset. The diamonds depict the linear mean α in each 2 dBZ range of Z, and the solid line is the regression to the diamonds.

best-fit line has the form

$$\log_{10}(\alpha) = 0.05017\,Z - 2.371, \tag{4}$$

where the units for α are m^{-1} and for Z are dBZ. The scatter of the data points is due principally to variations in mean particle size and represents a root-mean-square error on a retrieval of α of around $+200\%/-70\%$ for $Z \simeq -20$ dBZ, falling steadily to $+40\%/-30\%$ for $Z \simeq 0$ dBZ. In integrating retrieved extinction coefficients with height to obtain optical depth, one might expect the increase in mean size from cloud top to cloud base to introduce an independence in the errors in α at different altitudes, resulting in a somewhat more accurate estimate of optical depth. Nonetheless, we test the sensitivity to the scatter of the data by also calculating the optical depths using expressions that represent one standard deviation above and below the best-fit line of Eq. (4).

The principal remaining uncertainty lies in the choice of diameter in the Mie calculations to determine Z. The diameter D_m used here is commonly around 25% larger than the 'equivalent-area' diameter used in part I, and results in lower values of Z for the same particle mass because of the greater departure from Rayleigh scattering. This in turn leads to the retrieval of a larger value of extinction coefficient for a given measurement of Z. In consequence, the optical depth of cirrus is more likely to be overestimated than underestimated, resulting in a conservative estimate of how often any supercooled-water clouds observed by the lidar beneath the cirrus are radiatively important.

4. RESULTS

(a) *Frequency of occurrence of supercooled-water layers*

We first analyse the data collected at Chilbolton when the lidar was pointing $5°$ from zenith, which consists of essentially the whole of 2000, barring 12 January to 26 April when the instrument was taken off-line for repairs. In total, more than 700 000, 30 s rays were processed, equivalent to 248 days of continuous observation.
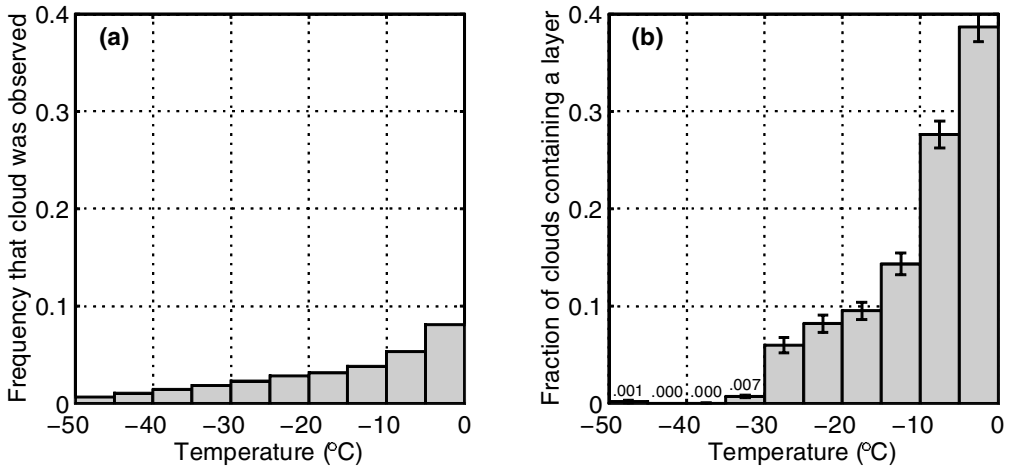
Figure 4.   Statistics of the occurrence of highly reflective layers attributable to liquid water in the data taken by the Chilbolton lidar ceilometer in 2000 when it was operating at 5° from zenith: (a) the fraction of observations in which cloud was seen in each 5 °C temperature interval (less than the true cloud occurrence due to extinction by intervening cloud); (b) the fraction of these clouds that contained a highly reflective layer.

The results are shown in Fig. 4. Panel (a) shows the fraction of the dataset for which the instrument observed any cloud in each 5 °C temperature interval between −50 °C and 0 °C. Hourly temperature profiles over Chilbolton were taken from the mesoscale version of the Met Office model. Pixels were defined to be cloudy if the lidar backscatter coefficient was 7.5×10^{-7} sr^{-1} m^{-1} or greater (the data were digitized in units of 2.5×10^{-7} sr^{-1} m^{-1}). To avoid contamination by boundary-layer aerosol, only data above 2 km were considered. An objective method was devised to 'clean up' the clear-air noise occasionally produced by this instrument. It can be seen that, except for the warmest bin, the occurrence of cloud in each 5 °C temperature interval was less than 5% and decreased with decreasing temperature. This is appreciably less than the true midlevel cloud occurrence over Chilbolton of around 20% (Hogan *et al.* 2001), because of the problem of lidar obscuration by lower-level clouds, particularly stratocumulus.

Figure 4(b) shows the fraction of the observed cloud (i.e. the fraction of cloudy rays) in each 5 °C interval that contained a supercooled liquid-water layer. The error bars were calculated assuming Poisson statistics, with every individual continuous layer being regarded as an independent event. Gaps of up to 10 min were permitted in layers for them still to be regarded as continuous, to allow for occasional obscuration by boundary-layer cumulus. As one might expect, the fraction of clouds containing a supercooled liquid-water layer decreased with decreasing temperature; 27% of clouds between −5 °C and −10 °C contained a supercooled layer, falling to 10% of clouds between −15 °C and −20 °C and 6% between −25 °C and −30 °C. Below −30 °C the frequency of occurrence falls suddenly, and below −40 °C, where liquid-water droplets are known to freeze spontaneously, a supercooled layer was diagnosed erroneously only once, and then only for 4.5 minutes.

Because the detection of one liquid-water layer by our algorithm precludes the detection of another in the same profile, the results were expressed as the fraction of clouds *in a given 5 °C temperature interval* that contain a layer, rather than the fraction of all clouds. Of course, one would expect the fraction of clouds containing a layer in a 10 °C interval to be proportionately greater than that for the 5 °C interval. It should also
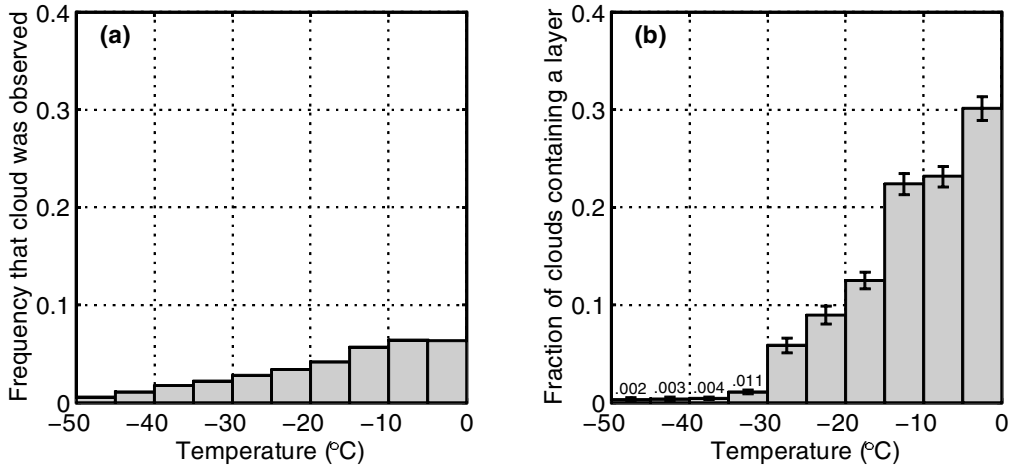
Figure 5.   Statistics of the occurrence of highly reflective layers in data taken by the Cabauw lidar operating at 5° from zenith.

be noted that the representation in Figs. 4(b) and 5(b) is not equivalent to the ratio of liquid-water content to total condensate that has been presented by authors such as Moss and Johnson (1994); due to the much smaller particle size, liquid water tends to be more radiatively effective than ice for the same water content, and our results are categorized by optical depth rather than water content.

Figure 5 shows similar statistics obtained by the lidar at Cabauw, also operating at 5° from zenith. The data were taken between October 2001 and July 2002, and the length of the dataset was equivalent to 287 days of continuous observation. Temperature profiles were extracted from the daily ECMWF model forecasts over the site. Panel (a) shows that the amount of cloud detected was not significantly different from Chilbolton. The frequency of occurrence of supercooled layers (shown in panel (b)) exhibits a similar decrease with decreasing temperature as observed at Chilbolton, but with a greater frequency between −20 and −10 °C, and a lower frequency between −10 and 0 °C. Of course, the climates of Chilbolton and Cabauw are very similar, and considerably more lidar data would need to be analysed to establish with confidence the extent to which supercooled-cloud occurrence varies with geographical location; a spaceborne lidar would be particularly suited to this purpose.

At this point we should question the representativity of these results even for the sites at which they were obtained, since no supercooled clouds can be detected by ground-based lidar in the presence of obscuring low-level liquid-water cloud. This immediately excludes important types of mixed-phase cloud from the statistics, most notably precipitating fronts. However, it should be pointed out that other techniques can also be susceptible to uneven sampling. For example, passive remote sensing from space only measures the phase of cloud top, while aircraft datasets (such as that analysed by Moss and Johnson (1994)) can inevitably contain a large but unrepresentative number of 'interesting' frontal systems to the exclusion of 'less interesting' clouds such as altocumulus, due to the fact that the decision on which clouds to sample is subjective. Therefore, we regard the statistics here as complementary to those obtained by other studies.
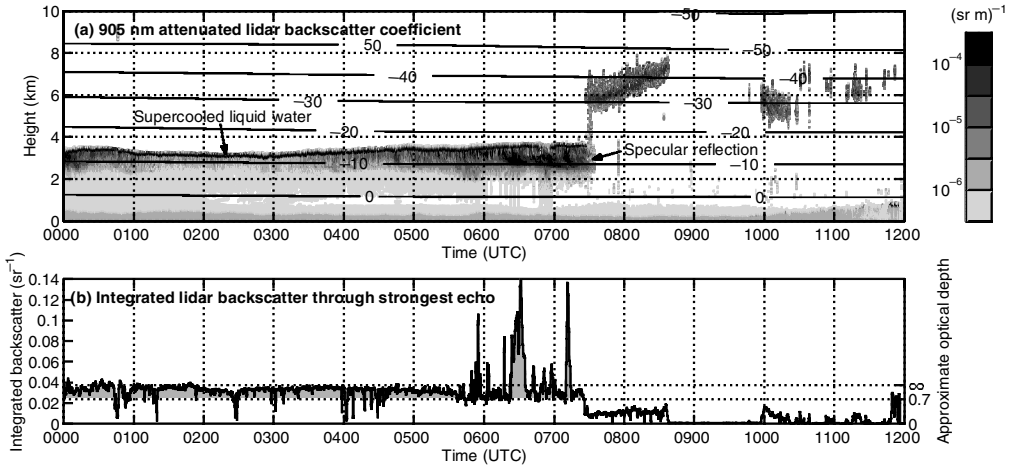
Figure 6. Example of specular reflection observed by zenith-pointing lidar at Chilbolton on 17 October 2002. As in Figs. 1 and 2, panel (b) depicts the integrated backscatter in a 300 m vertical window encompassing the strongest echo. The temperature contours were obtained by interpolating in time between four radiosonde ascents from Larkhill, 25 km to the west of Chilbolton.

(b)   Specular reflection from horizontally aligned plate crystals

To demonstrate the problems that can be experienced by the algorithm when it is applied to data taken by lidar pointing directly at zenith, Fig. 6 shows a 12 h section of β' (panel (a)) and γ_w (panel (b)) in an altocumulus cloud observed at zenith. Until around 0530 UTC, the strongest echo was from the $-15\,^\circ$C liquid layer at cloud top, where γ_w approached the asymptote corresponding to an infinite optical depth, as in Figs. 1 and 2. From 0530 to 0730 UTC, however, the strongest backscatter was intermittently to be found 500–1000 m below the liquid-water layer, and here γ_w exceeded the theoretical asymptotic value by more than a factor of three. This indicates that the enhanced backscattered echo was not accompanied by any significant increase in extinction, i.e. that k had a very low value. The same phenomenon was observed by Platt (1977), who attributed it to specular reflection from horizontally aligned plate crystals. It, therefore, does not indicate any significant enhancement of the radiative importance of the ice, and is not observed in data taken away from zenith. It is our experience that this phenomenon tends to occur most often beneath liquid-water layers, which is consistent with the observations in part I of high differential reflectivity beneath supercooled-liquid layers, indicating the presence of horizontally aligned, high-density pristine crystals.

Figure 7 shows the statistics for cloud detection and supercooled-water occurrence obtained for the Chilbolton lidar between 22 April and 30 November 1999, when it was pointing at zenith. Again, temperature was obtained from the Met Office model. Comparing Fig. 7(b) with Fig. 4(b) it can be seen that the effect of specular reflection is to increase the fraction of clouds containing a layer by 0.05–0.1 between $-20\,^\circ$C and $-10\,^\circ$C, which is precisely the region where one would expect plate crystals to exist. At other temperatures the occurrence is generally very similar.

(c)   Horizontal extent of supercooled-water layers

Figure 8(a) shows the mean layer duration as a function of mean layer temperature, for the three datasets presented in Figs. 4, 5 and 7. The value plotted is actually the
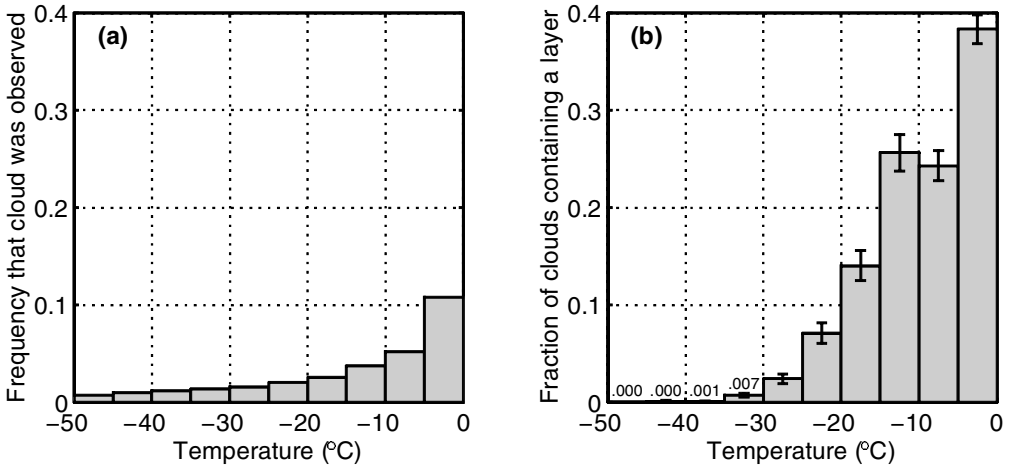
Figure 7.   Statistics of the occurrence of highly reflective layers in data taken by the Chilbolton lidar in 1999 when it was operating at zenith.
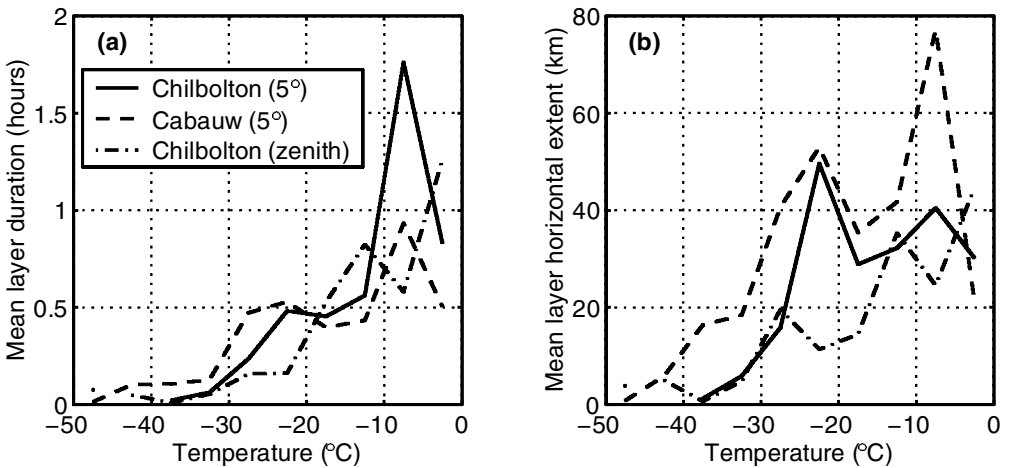

Figure 8.   Mean duration and horizontal extent of individual layers versus temperature, for the three datasets shown in Figs. 4, 5 and 7.

'expected value' of the duration of a layer, *given that a layer has been detected.* This way the mean is weighted towards the long-lived clouds that contribute most to the total fraction of clouds containing a supercooled layer, rather than being weighted towards the numerous small clouds that persist for only a few minutes but do not contribute significantly to the total. Because of the frequent temporary obscuration of the layers by passing low-level cumulus, layers were deemed continuous in this analysis if any gaps in them lasted no longer than 10 minutes, although it is recognized that the resulting layer durations may still be underestimated because of the possibility of obscuration for periods longer than 10 min.

Horizontal extent was calculated from layer duration using the wind speed over the site, from the Met Office model in the case of Chilbolton, and from the ECMWF model in the case of Cabauw. It can be seen that the mean horizontal extent of layers warmer
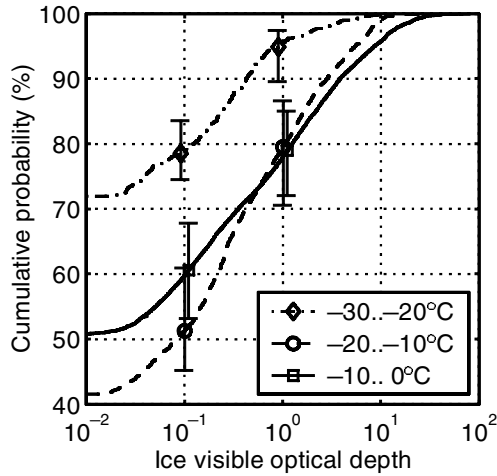
Figure 9. Cumulative probability distribution of the optical depth of the ice cloud above layers of supercooled water in three different temperature ranges. The observations used were from Chilbolton in 2000, when the lidar was operated at $5°$ from zenith to avoid specular reflection from aligned crystals.

than $-30\,°C$ observed at $5°$ from zenith typically varied between 20 and 70 km, with a tendency for more extensive layers over Cabauw than Chilbolton. The layers observed at zenith appear to have been somewhat less horizontally extensive on average. At temperatures below $-30\,°C$, the few layers that were detected by the algorithm typically persisted for less than 6 min.

(d) Optical depth of cirrus above supercooled-water layers

We next use radar reflectivity to estimate the optical-depth distribution of the ice cloud overlaying the supercooled liquid-water clouds. Chilbolton data are analysed from 2000 when the lidar operated in an off-zenith configuration, in order to be confident that almost all the highly reflective layers observed were composed of liquid water. The Galileo radar was available until 17 October 2000, and the lidar was available for the whole year except 12 January to 26 April, leaving 147 days in which radar, lidar and model data were available. Layers were diagnosed from the lidar β' profile as before, and the optical depth of any cirrus above them was found by integrating the extinction coefficient derived from Z up from the height of the layer to the highest radar echo.

The results are shown in Fig. 9, divided according to the temperature of the supercooled cloud. It is found that around 20% of supercooled clouds between $0\,°C$ and $-20\,°C$ had ice cloud above with an optical depth in excess of 1, falling to 5% of supercooled clouds between $-20\,°C$ and $-30\,°C$. These values increase when ice optical depths of greater than 0.1 are considered, lying between 20% and 50% depending on the temperature. The error bars of up to $\pm10\%$ indicate the range of uncertainty associated with the use of radar reflectivity to estimate ice optical depth, as discussed in section 3(c). The same analysis was performed on the 196 days of 1999 for which radar, lidar and model data were available, and the results were very similar.

The radiative-transfer calculations performed in part I suggested that in cloud profiles containing both liquid water and ice, the supercooled liquid water would have a stronger net effect on the radiation budget than the ice for ice optical depths of up to around 1, in the daytime. By considering only the long-wave flux reported in part I, we estimate that at night the supercooled water has a stronger effect only when any

ice above has an optical depth of less than approximately 0.1. Therefore, the results presented here indicate that, when present, supercooled liquid water will dominate the radiative properties of a cloud profile in over 80% of daytime cases, and in more than half of night-time cases.

The relatively low sensitivity of the radar in the last few months of the dataset means that some radiatively significant ice cloud may not have been detected, particularly in the upper troposphere. Therefore, the fraction of supercooled clouds that dominate the radiative properties of the cloud profile may be overestimated. Conversely, there will be occasions when the lidar sees only the lowest of several liquid-water layers embedded within an ice cloud, in which case the relative importance of the ice will be overestimated. A particular example of this is the mixed-phase cloud observed by airborne lidar on 20 October 1998 in part I, which contained four individual liquid-water layers. The coldest layer occurred at the top of the midlevel cloud, yet for the ground-based lidar it was completely obscured by the lowest of the layers 2 km below.

(e) Comparison of observed occurrence of supercooled water with values in the ECMWF and UK Met Office models

In this section we compare the observed occurrence of supercooled water at Chilbolton by lidar pointing $5°$ from zenith (Fig. 4(b)) with the occurrence in a year of data from both the ECMWF model and the mesoscale version of the Met Office Unified Model over Chilbolton. The model data are taken from April 1999 to March 2000 inclusive. The models are rather different in the way they represent cloud; the Met Office model carries separate prognostic variables for ice content and liquid/vapour content, the division between liquid and vapour being diagnosed mainly from temperature (Smith 1990), while the ECMWF model has separate prognostic variables for vapour and condensed water, with the ice/liquid-water ratio being diagnosed purely as a function of temperature (Matveev 1984).

We apply the same 0.7 optical-depth threshold in the model as in the observations. The effective radius of liquid-water clouds over land is 10 μm in the ECMWF model (J.-J. Morcrette, personal communication), so a model layer is deemed to contain a layer if the liquid-water path of the cloudy part of the grid box (calculated using the model cloud fraction) exceeds 4.7 g m^{-2}. The Met Office used a constant value of 7 μm over land until 12 October 1999, after which they moved to a parametrization in which the number concentration of droplets was kept constant and the size was allowed to change (J. M. Edwards, personal communication). For consistent analysis of the Met Office model data, we assume a constant value of 7 μm for the whole period, which equates to a critical liquid-water path of 3.3 g m^{-2}. Grid boxes with a cloud fraction of less than 0.05 are rejected from the analysis.

Figure 10 shows the fraction of model clouds in each 5 $°$C temperature interval that contain significant liquid water, with the observations from Fig. 4(b) depicted by the superimposed error bars. The comparison clearly indicates that supercooled liquid water in the models tends to occur too frequently at warmer temperatures and too infrequently at colder temperatures, although the occurrence was considerably more in the ECMWF model than in the Met Office model. Neither model contained significant liquid water at temperatures below -20 $°$C, although in the case of the ECMWF model, the diagnostic ice/liquid ratio does not allow liquid to exist at temperatures below -23 $°$C.

The clouds in the Met Office model were also found to contain supercooled liquid water around 25% more frequently in the winter than the summer (not shown). This could be because stratocumulus, which is common throughout the year, is more likely
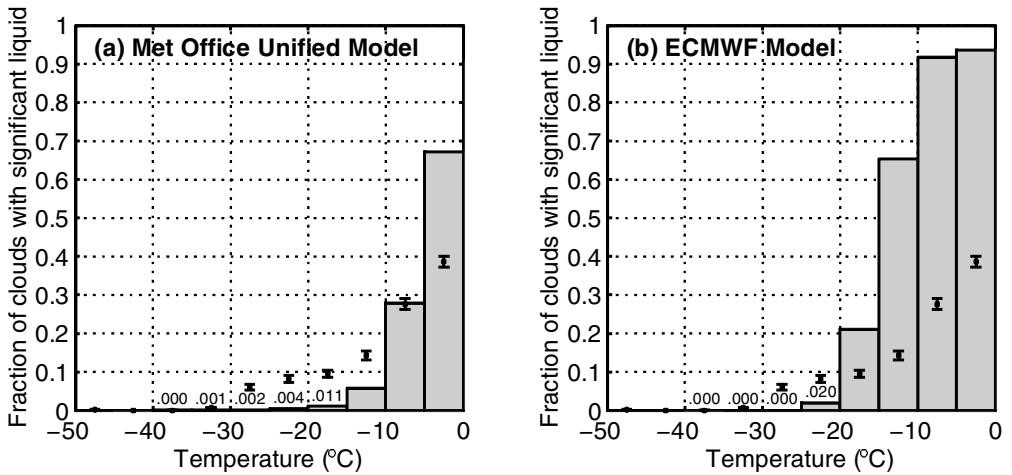
Figure 10.   The grey bars depict the frequency of supercooled-water clouds over Chilbolton in (a) the mesoscale version of the UK Met Office model and (b) the ECMWF model. The superimposed error bars show the observed values, taken from Fig. 4(b).

to be supercooled in winter, although no similar trend was evident in the lidar observations. The ECMWF model with its diagnosed liquid/ice fraction exhibited no seasonal dependence.

A number of factors could contribute to the difference between the observations and the models. In the case of the models, the 500–750 m vertical resolution in the midtroposphere would certainly make it difficult to simulate supercooled clouds anything like those observed with lidar, which are typically only 150 m thick. Also, the model does not represent the subgrid-scale fluctuations in vertical velocity that in part I were suggested to be responsible for the condensation of liquid water. On the other hand, the representativeness of the observations is questionable because they exclude the majority of fronts due to obscuration by low-level cloud, yet the mixed-phase cloud scheme in the Met Office model was formulated principally with fronts in mind.

5. CONCLUSIONS

A first attempt was made to characterize the frequency of occurrence of stratiform supercooled liquid-water clouds as a function of temperature by utilizing the fact that liquid water tends to be strikingly visible in lidar imagery as highly reflective layers apparently around 150 m thick. An algorithm was developed that utilizes the integrated backscatter to identify occurrences of supercooled liquid water with an optical depth greater than 0.7. Between $-5\,^{\circ}$C and $-10\,^{\circ}$C, around 27% of clouds at Chilbolton were found to contain a supercooled liquid-water layer, the probability falling steadily with temperature to essentially zero below $-35\,^{\circ}$C. Operating at zenith was found to bias the statistics between $-20\,^{\circ}$C and $-10\,^{\circ}$C, due to specular reflection from horizontally aligned plate crystals at this temperature. It should be noted that these results may not be representative of all types of mixed-phase clouds since obscuration by low cloud means that they unavoidably exclude precipitating frontal systems and deep convection. They are also restricted to one particular climatic zone.

Concurrent radar observations suggested that less than half of the layers had ice above them with an optical depth of more than 0.1, and less than 20% had ice above

with an optical depth greater than 1. Given the significant optical depths of the layers themselves, and considering the radiative-transfer calculations performed in part I, this demonstrates that in the majority of cases where supercooled water is present it dominates the radiative properties of the cloud profile, and therefore is likely to be important for climate.

Many forecast and climate models still parametrize mixed-phase clouds using a simple ratio between liquid- and ice-water content which varies with temperature alone, but in part I it was shown that mixed-phase clouds are far from being homogeneously mixed. Altocumulus was commonly observed in the ground-based lidar data used in this paper, and consists of a thin liquid-water layer beneath which ice is falling (see also the 21 October 1998 case in part I); this scenario of liquid over ice cannot be simulated by such models. Figure 10 indicates that the temperature dependence of the fraction of clouds containing radiatively significant liquid water is considerably in error. Before these findings can be used to improve models one must determine the underlying causes of the phenomenon that could be used as a basis for parametrization, and whether any of the more sophisticated microphysical parametrizations already in existence have any skill. A first step would be to compare individual instances of supercooled cloud with model parameters such as vertical velocity, stability, humidity and Richardson number. However, we would not expect good representation of thin liquid layers in models until vertical resolutions in the midtroposphere are improved. Work to simulate these clouds in a cloud-resolving model is currently in progress.

Comparison of these ground-based results with the POLDER satellite measurements discussed in the introduction reveals some agreements but raises questions. The lidar/radar studies suggest a steady decrease in the occurrence of liquid water with temperature as reported by Giraud *et al.* (2001), rather than the step change at $-33\,^\circ$C inferred by Riedi *et al.* (2001). However, Giraud *et al.* (2001) suggest that the large brightness-temperature differences observed between 11 and 12 μm, previously ascribed to semi-transparent cirrus (Inoue 1985) are in fact indicative of semi-transparent liquid-water clouds, arising because the refractive index of liquid-water cloud is also higher at 12 μm than 11 μm. The lidar data presented here do not support this hypothesis as the layers detected are by no means semi-transparent; indeed, the principal criterion for their identification is that they have a high backscatter coefficient, which implies that they are optically thicker than any ice cloud of the same physical thickness is likely to be. This ties in with the suggestion of Heymsfield *et al.* (1991) that supercooled altostratus clouds are physically similar to stratocumulus, since stratocumulus clouds certainly tend not to be semi-transparent. It would, therefore, be very interesting to compare ground-based lidar observations directly with cloud phase inferred from POLDER or other passive spaceborne instruments, such as the Moderate Resolution Imaging Spectroradiometer (MODIS); see Strabala *et al.* (1994) and Baum *et al.* (2000).

The National Aeronautics and Space Administration are currently planning the launch of 'Calipso', a spaceborne-lidar mission specifically for monitoring clouds and aerosols; its ability to locate supercooled-water clouds will provide a global dataset with which it will be possible to evaluate the various passive techniques for cloud-phase detection, test the representation of cloud phase in numerical models, and assess the overall climatological importance of supercooled-water clouds in the atmosphere.

REFERENCES

Baum, B. A., Soulen, P. F., Strabala, K. L., King, M. D., Ackerman, S. A., Menzel, W. P. and Yang, P. — 2000 — Remote sensing of cloud properties using MODIS airborne simulator imagery during SUCCESS. 2. Cloud thermodynamic phase. *J. Geophys. Res.*, **105**, 11781–11792

Brown, P. R. A. and Francis, P. N. — 1995 — Improved measurements of the ice water content in cirrus using a total-water probe. *J. Atmos. Oceanic Technol.*, **12**, 410–414

Brown, P. R. A., Illingworth, A. J., Heymsfield, A. J., McFarquhar, G. M., Browning, K. A. and Gosset, M. — 1995 — The role of spaceborne millimeter-wave radar in the global monitoring of ice-cloud. *J. Appl. Meteorol.*, **34**, 2346–2366

Eloranta, E. W. — 1998 — A practical model for the calculation of multiply scattered lidar returns. *Appl. Opt.*, **37**, 2464–2472

Francis, P. N., Hignett, P. and Macke, A. — 1998 — The retrieval of cirrus cloud properties from aircraft multi-spectral reflectance measurements during EUCREX'93. *Q. J. R. Meteorol. Soc.*, **124**, 1273–1291

Gibson, A. J., Thomas, L. and Bhattacharyya, S. K. — 1977 — Some characteristics of cirrus clouds deduced from laser radar observations at different elevation angles. *J. Atmos. Terr. Phys.*, **29**, 657–660

Giraud, V., Thouron, O., Riedi, J. and Goloub, P. — 2001 — Analysis of direct comparison of cloud top temperature and infrared split window signature against independent retrievals of cloud thermodynamic phase. *Geophys. Res. Lett.*, **28**, 983–986

Goloub, P., Herman, M., Chepfer, H., Riedi, J., Brogniez, G., Couvert, P. and Seze, G. — 2000 — Cloud thermodynamical phase classification from the POLDER spaceborne instrument. *J. Geophys. Res. Atmos.*, **105**, 14747–14759

Gregory, D. and Morris, D. — 1996 — The sensitivity of climate simulations to the specification of mixed phase clouds. *Clim. Dyn.*, **12**, 641–651

Heymsfield, A. J., Miloshevich, L. M., Slingo, A., Sassen, K. and Starr, D. O'C. — 1991 — An observational and theoretical study of highly supercooled altocumulus. *J. Atmos. Sci.*, **48**, 923–945

Hogan, R. J. and Illingworth, A. J. — 1999 — The potential of spaceborne dual-wavelength radar to make global measurements of cirrus clouds. *J. Atmos. Oceanic Technol.*, **16**, 518–531

Hogan, R. J., Jakob, C. and Illingworth, A. J. — 2001 — Comparison of ECMWF cloud fraction with radar-derived values. *J. Atmos. Oceanic Technol.*, **40**, 513–525

Hogan, R. J., Bouniol, D., Ladd, D. N., O'Connor, E. J. and Illingworth, A. J. — 2003a — Absolute calibration of 94/95-radars using rain. *J. Atmos. Oceanic Technol.*, **20**, 572–580

Hogan, R. J., Francis, P. N., Flentje, H., Illingworth, A. J., Quante, M. and Pelon, J. — 2003b — Characteristics of mixed-phase clouds. I: Lidar, radar and aircraft observations from CLARE'98. *Q. J. R. Meteorol. Soc.*, **129**, 2089–2116

Inoue, T. — 1985 — On the temperature and effective emissivity determination of semi-transparent cirrus clouds by bi-spectral measurements in the 10 micron window region. *J. Meteorol. Soc. Jpn*, **63**, 88–99

Liebe, H. J.	1985	An updated model for millimeter-wave propagation in moist air. *Radio Sci.*, **20**, 1069–1089
McFarquhar, G. M. and Heymsfield, A. J.	1997	Parameterization of tropical cirrus ice crystal size distributions and implications for radiative transfer: Results from CEPEX. *J. Atmos. Sci.*, **54**, 2187–2200
Matveev, L. T.	1984	*Cloud Dynamics.* D. Reidel
Moss, S. J. and Johnson, D. W.	1994	Aircraft measurements to validate and improve numerical model parametrizations of ice to water ratios in clouds. *Atmos. Res.*, **34**, 1–25
Pinnick, R. G., Jennings, S. G., Chylek, P., Ham, C. and Grandy, W. T.	1983	Backscatter and extinction in water clouds. *J. Geophys. Res.*, **88**, 6787–6796
Platt, C. M. R.	1973	Lidar and radiometric observations of cirrus clouds. *J. Atmos. Sci.*, **30**, 1191–1204
	1977	Lidar observation of a mixed-phase altostratus cloud. *J. Appl. Meteorol.*, **16**, 339–345
Platt, C. M. R., Abshire, N. L. and McNice, G. T.	1978	Some microphysical properties of an ice cloud from lidar observation of horizontally oriented crystals. *J. Appl. Meteorol.*, **17**, 1220–1224
Riedi, J., Goloub, P. and Marchand, R. T.	2001	Comparison of POLDER cloud phase retrievals to active remote sensor measurements at the ARM SGP site. *Geophys. Res. Lett.*, **28**, 2185–2188
Sassen, K.	1984	Deep orographic cloud structure and composition derived from comprehensive remote sensing measurements. *J. Clim. Appl. Meteorol.*, **23**, 568–583
	1991	The polarization lidar technique for cloud research—a review and current assessment. *Bull. Am. Meteorol. Soc.*, **72**, 1848–1866
Smith, R. N. B.	1990	A scheme for predicting layer clouds and their water content in a general circulation model. *Q. J. R. Meteorol. Soc.*, **116**, 435–460
Strabala, K. I., Ackerman, S. A. and Menzel, W. P.	1994	Cloud properties inferred from 8–12-μm data. *J. Appl. Meteorol.*, **33**, 212–229
Sun, Z. and Shine, K. P.	1995	Parameterization of ice cloud radiative properties and its application to the potential climatic importance of mixed-phase clouds. *J. Climate*, **8**, 1874–1888
Thomas, L., Cartwright, J. C. and Wareing, D. P.	1990	Lidar observations of the horizontal orientation of ice crystals in cirrus clouds. *Tellus*, **42B**, 211–216
Tremblay, A., Glazer, A., Yu, W. and Benoit, R.	1996	A mixed-phase cloud scheme based on a single prognostic equation. *Tellus A*, **48**, 483–500
Wilson, D. R. and Ballard, S. P.	1999	A microphysically based precipitation scheme for the UK Meteorological Office Unified Model. *Q. J. R. Meteorol. Soc.*, **125**, 1607–1636